1	Super-selective Removal of Lead from Water by Two-Dimensional
2	MoS ₂ Nanosheets and Layer-stacked Membranes
3	
4	Research article
5	Revision Submitted to
6	Environmental Science & Technology
7	
8	Zhongying Wang, ^{1,2} ** Qingsong Tu ³ *, Alison Sim¹, Julie Yu¹, Yanghua
9	Duan ¹ , Sidney Poon ¹ , Bei Liu ² , Qi Han ² , Jeffrey J. Urban ⁴ , David Sedlak ¹ , and
10	Baoxia Mi ¹ *
11 12	¹ Department of Civil and Environmental Engineering, University of California, Berkeley, California 94720, United States
13 14 15	² Guangdong Provincial Key Laboratory of Soil and Groundwater Pollution Control, School of Environmental Science and Engineering, Southern University of Science and Technology, 1088 Xueyuan Blvd, Nanshan District, Shenzhen 518055, PR China
16 17	³ Materials Sciences Division, Lawrence Berkeley National Laboratory, Berkeley, California 94720, United States
18 19	⁴ The Molecular Foundry, Lawrence Berkeley National Laboratory, Berkeley, California 94720, United States
20	*The author to whom correspondence should be addressed.
21	# The author contributed equally to the work.

E-mail: mib@berkeley.edu; wangzy6@sustech.edu.cn

Abstract

24

25

26

27

28

29

30

31

32

33

34

35

36

37

38

Point-of-use (POU) devices with satisfactory lead (Pb²⁺) removal performance are urgently needed in response to recent outbreaks of lead contamination in drinking water. This study experimentally demonstrated the excellent lead removal capability of two-dimensional (2D) MoS₂ nanosheets in aqueous form and as part of a layer-stacked membrane. Among all materials ever reported in the literature, MoS₂ nanosheets exhibit the highest adsorption capacity (740 mg/g), and the strongest selectivity/affinity towards Pb^{2+} with a distribution coefficient K_d that is orders of magnitude higher than that of other lead adsorption materials (5.2×10⁷ mL/g). Density functional theory (DFT) simulation was performed to complement experimental measurements and to help understand the adsorption mechanisms. The results confirmed that the cation selectivity of MoS₂ follows the order $Pb^{2+} > Cu^{2+} > Cd^{2+} > Zn^{2+}$, $Ni^{2+} > Mg^{2+}$, K^+ , Ca^{2+} . The membrane formed with layer-stacked MoS₂ nanosheets exhibited a high water flux (145 L/m²/h/bar), while effectively decreasing Pb²⁺ concentration in drinking water from a few mg/L to less than 10 µg/L. The removal capacity of the MoS₂ membrane is a few orders of magnitude higher than that of other literature-reported membrane filters. Therefore, the layer-stacked MoS₂ membrane has great potential for POU removal of lead from drinking water.

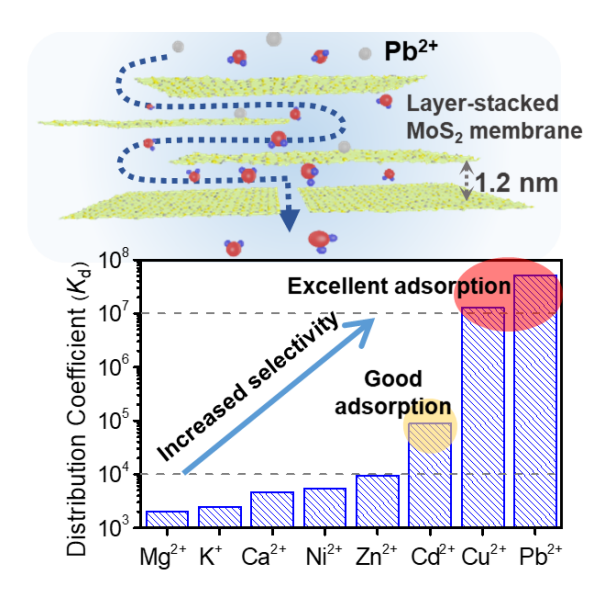
40

41

39

- KEYWORDS: layer-stacked MoS₂ membrane; point-of-use device; lead contamination; drinking
- water; super-selective adsorption; high adsorption capacity

44 Table of Contents (TOC)



INTRODUCTION

47

48

49

50

51

52

53

54

55

56

57

58

59

60

61

62

63

64

65

66

67

68

69

Toxic heavy metal contamination of freshwater and drinking water has become a critical challenge for human society. Particularly, lead (Pb²⁺) has been recognized as one of the most toxic metals worldwide and there have been cases of lead contamination of tap water in various cities (e.g., Washington, DC; Flint, MI; and Newark, NJ) in the United States. A major source of lead in drinking water is the lead-containing plumbing in water distribution systems like pipes, solders, and fittings. As aged lead-containing pipelines are still used, lead concentrations can be on the order of tens of milligrams per liter in the aftermath of man-made mismanagement or natural disasters.^{1, 2} This is several orders of magnitude higher than the U.S. EPA lead action level (15 μg/L) and the WHO guideline value (10 μg/L).^{3, 4} Long-term exposure to lead, even at extremely low concentrations, increases the blood lead level due to its bio-accumulative nature, causing severe adverse health effects in the nervous system and brain, particularly in infants and children.⁵ To remove lead from drinking water, especially for daily-use in rural areas or for responding to emergency lead contamination incidents, portable point-of-use (POU) adsorption technologies are essential because of their flexibility, ease of operation, and cost effectiveness. Some promising adsorbents targeting heavy metal remediation have been recently identified, including metal-organic frameworks (MOFs),^{6, 7} graphene-based materials,⁸ covalent organic frameworks, 9, 10 layered nanomaterials 11-14, and natural materials like biochar 15. However, sorption materials that have ultrahigh affinity and selectivity to lead are still lacking. High selectivity is extremely important because one challenge hindering effective removal of lead from drinking water is the presence of interfering species. In addition, the adsorption materials used in POU applications should possess attributes such as high porosity, adsorption-site accessibility, and homogeneous binding sites to achieve fast kinetics and high capacity.

Two-dimensional (2D) molybdenum disulfide (MoS₂), one of the most widely researched transition metal dichalcogenides (TMDs), is an ideal adsorbent material for heavy metal remediation because of its large surface area, and is abundant active sulfur sites that have a high affinity to heavy metals. Although MoS₂ is a naturally occurring mineral, the direct use of bulk MoS₂ in heavy metal remediation is impossible because the interlayer spacing (0.63 nm) is so small that targeted heavy metal ions are unable to access the interior sulfur atoms. Synthetic 2D MoS₂ nanomaterials (*e.g.*, flower-like aggregates) have been explored as adsorbents for toxic transition metal (Hg²⁺, Pb²⁺, Ag⁺, Zn²⁺, Cd²⁺) remediation, showing moderate-to-high adsorption capacities ¹⁸⁻²⁵. However, little investigation has been done to quantify the affinity and selectivity of MoS₂-based adsorbents. The surface area of MoS₂ available for adsorption is also compromised due to the aggregation of MoS₂ nanosheets during hydrothermal synthesis. In contrast, the exfoliated MoS₂ monolayers possess the highest theoretical surface area. However, limited work has been done investigating its application as an adsorbent in a POU device for lead ion removal.

To address the above research needs, we systematically studied the adsorption of Pb²⁺ by MoS₂ monolayers and the effects of interfering ions and compared its selectivity and capacity to that of other heavy metal ions. Batch tests and DFT simulations were used to unveil the selectivity and adsorption mechanisms of MoS₂ towards various ions. The layer-stacked MoS₂ structure with confined and ordered nanochannels was employed as a POU filter, and its performance and mechanism for removing Pb in continuous filtration was investigated to reveal the potential in practical applications.

MATERIALS AND METHODS

MoS₂ nanosheets,²⁷ 5 ml of 1.6 M n-butyllithium in hexane solution was added to ~500 mg of bulk MoS₂ powder (~ 2 μm, Sigma-Aldrich), and the mixture was was kept at room temperature for 2 d in a nitrogen-filled glovebox with mild stirring. The resulting lithium-intercalated product was rinsed with hexane to remove organic reactants and by-products. The purified intercalated product was immediately exfoliated by reaction with DI water in an ultrasonic bath for 1 h. MoS₂ nanosheets well-dispersed in solution were obtained after dialysis of the dispersion against DI water to remove inorganic byproduct LiOH. The total MoS₂ concentration was determined through digestion in 0.2 M HNO₃ and 0.5 M H₂O₂ solution, followed by measurement of the soluble Mo species concentration in ICP-OES (Agilent 720, Agilent Technologies, Santa Clara, CA). Dispersions of chemically exfoliated MoS₂ samples were stored in 4 °C for further use. To prepare layer-stacked MoS₂ membranes, a dispersion containing 4 mg MoS₂ was filtered through a polyethersulfone (PES) ultrafiltration membrane with a nominal pore size of 30 nm (Sterlitech, Kent, WA), generating an MoS₂ membrane with a thickness of ~ 600 nm.

Metal ion adsorption by suspended MoS2 nanosheets. Metal cation adsorption by MoS2 nanosheets was studied in batch experiments. The metal cations tested include Mg²⁺, K⁺, Ca²⁺, Ni²⁺, Cd²⁺, Zn²⁺, Cu²⁺ and Pb²⁺ in their nitrate salt forms. After mixing MoS2 nanosheets (100 mg/L) with individual cations (~ 5 mg/L) in 10 mL buffer solutions (MES, 10 mM, pH 6) for 1 d, cation-adsorbed nanosheets were removed through 0.22 µm PES syringe filters (VWR), and the cation concentrations in the filtrate solutions were determined using ICP-OES or ICP-MS (Agilent 7700 Series) for low concentration (≤ 10 µg/L). The removal is calculated as $R = 100 \times (C_0 - C_f)/C_0$ %, where C_0 and C_0 are the initial and final cation concentrations (mg/L), respectively. The distribution coefficient is calculated as $K_d = (V[(C_0 - C_f)/C_f])/m$, where V is the solution volume

(mL), and m is the adsorbent mass (g).

116

117

118

119

120

121

122

123

124

125

126

127

128

129

130

131

132

133

134

135

136

137

138

To characterize the competitive adsorption of metal cations, batch experiments were carried out with a mixed solution containing ~5 mg/L of each cation (Mg²⁺, K⁺, Ca²⁺, Ni²⁺, Cd²⁺, Zn²⁺, Cu²⁺ and Pb²⁺) and 100 mg/L MoS₂ nanosheets. A solution mimicking tap water composition was prepared by spiking DI water with NaCl (280 mg/L), CaCl₂ (150 mg/L) and MgSO₄ (75 mg/L). Batch tests were also used to understand the Pb²⁺ removal capacity, kinetics, and selectivity. In order to test the regeneration capability of MoS₂, we used a strong chelating agent EDTA, which has a Pb-EDTA²⁻ formation constant of approximately 10¹⁸ to recover Pb from MoS₂. In each repeated test, 50 mg/L Pb²⁺ and 100 mg/L MoS₂ was added to 40 mL of pH 6 buffer solution, and the sample was then mixed for 2 h before the solid Pb-MoS2 was collected by vacuum-filtration onto a PES membrane. To recover the MoS2, 40 mL of 5 mM EDTA solution was added to the collected Pb-MoS₂ to allow the release of Pb from MoS₂ for 2 h, then the regenerated MoS₂ was recollected by vacuum filtration for use in the next cycle. Pb removal by layer-stacked MoS₂ membranes. The filtration experiments were performed using a dead-end stirred cell filtration system (Model 8050, EMD Millipore) with a total internal volume of 50 mL and an active surface area of 13 cm². The solution in the chamber was continuously mixed with a suspended magnetic stirrer at 200 rpm. The chamber was filled with aqueous solution containing Pb2+ at various concentrations (0.25, 1, 3 mg/L), which was continuously supplied from a stock solution in a plastic container. The filtration experiments were started by applying ~ 10 psi pressure to the chamber by means of compressed N₂. Ten-mL samples of the filtrate were periodically collected and analyzed by ICP-MS. Density functional theory (DFT) simulations. All simulation results were calculated using DFT software VASP.²⁸ The exchange-correlation functional was described using generalized gradient approximation (GGA) with Perdew-Burke-Ernzerhof (PBE),²⁹ and the ion-electron interaction was treated with the projector augmented wave (PAW) method.³⁰ The cutoff energy was 520 eV and the energy convergence criterion was 10⁻⁵ eV/cell. The conjugate gradient method was adopted for the geometry optimization. The Brillouin zone was represented by a Monkhorst–Pack special k-point mesh³¹ of different sizes depending on the MoS₂ size. For all calculations, the van der Waals (vdW) interaction was included using a dispersion correction term from the DFT-D3 method.³² A large vacuum space of 30 Å was used to avoid any interaction of the MoS₂ sheets with their images. The electron localization function (ELF) calculation was also performed for detailed data analysis.³³ ELF is derived from the calculation of Pauli repulsion with values normalized between 0 and 1.³⁴ Notably, the Hubbard U correction was not added here since little changes were found for the electronic structure of MoS₂ in previous studies.³⁵⁻³⁸

Material and membrane characterization. MoS₂ nanosheets were characterized through transmission electron microscopy (TEM), atomic force microscopy (AFM), and X-ray photoelectron spectroscopy (XPS). TEM images were obtained with a JEM-2100F. The AFM

155 Grinstead156 (Malvern

Grinstead, UK). The zeta potential measurement was performed on a Zetasizer Nano-ZSP analyzer

(Malvern, Westborough, MA). Cross-sectional images of a layer-stacked MoS₂ were recorded by

images were obtained in air using a Bruker Dimension Icon in tapping mode. The XPS

measurement was conducted with a K-Alpha XPS spectrometer (Thermo Scientific Ltd, East

a field emission SEM (Zeiss Gemini Ultra-55, Jena, Germany).

RESULTS AND DISCUSSION

Synthesis of MoS₂ nanosheets and layer-stacked membranes. We prepared MoS₂ monolayer nanosheets from MoS₂ bulk material through chemical exfoliation, ^{27,39} engineered them into layer-

stacked membranes, and tested the Pb removal by both configurations of MoS₂ (Figure 1a-c). The as-prepared MoS₂ nanosheets were highly dispersible in water because of their uniformly distributed negative charge on the surface (*e.g.*, each MoS₂ unit cell is believed to carry -0.25 eV),⁴⁰ as confirmed by a zeta potential of -40 to -50 mV in a wide pH range (Figure S1a). According to the TEM (Figure S1b) and AFM (Figure 1d) images, a majority of the exfoliated MoS₂ nanosheets had a lateral dimension of 100 to 500 nm and a monolayer thickness of ~1.1 nm. The phase composition of MoS₂ nanosheets characterized by XPS (Figure S1c-d) consisted of 40% 2H-MoS₂ and 60% 1T-MoS₂, which is consistent with the results of exfoliation-induced phase transformation reported previously.³⁹ Layer-stacked MoS₂ membranes were fabricated by filtration leading to a stable interlayer spacing of ~ 1.2 nm, which was naturally formed and stabilized by a balance between attractive van der Waals and repulsive hydration forces according to our previous study.⁴¹ In this stacked configuration, MoS₂ membranes maintain an ultrahigh surface area, exposing all sulfur atoms on each nanosheet as accessible metal-binding sites, and thus potentially enabling a POU device with continuous water flow as well as high metal adsorption capacity.

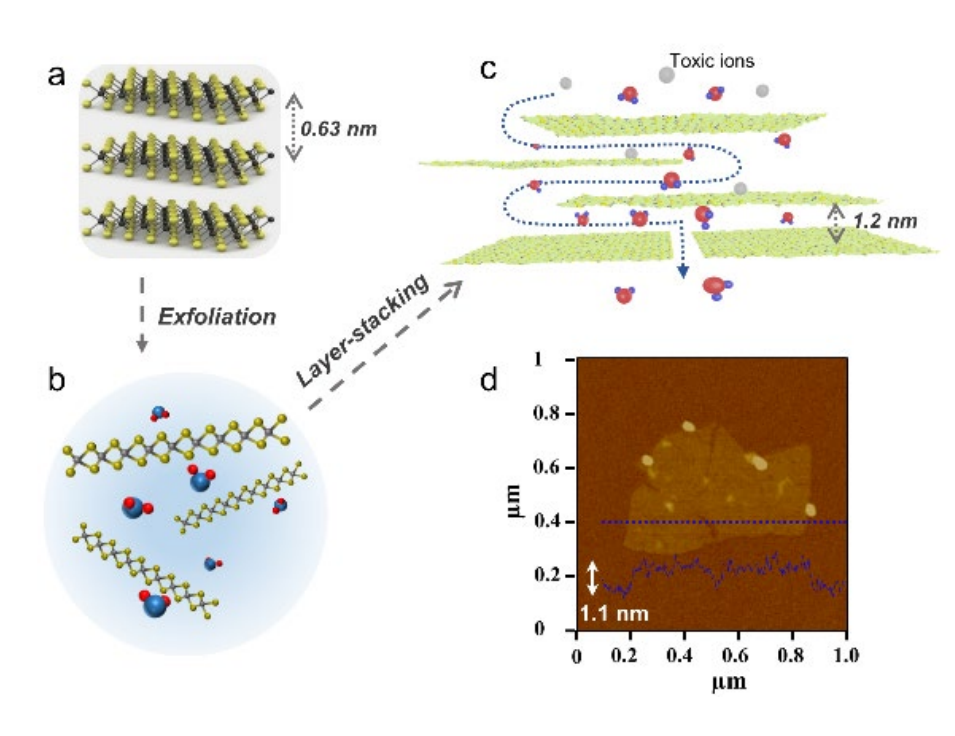


Figure 1. Schematic illustration of exfoliating bulk MoS₂ materials (a) to create an aqueous suspension of

MoS₂ monolayer nanosheets (b) and reassembling the nanosheets into a layer-stacked MoS₂ membrane (c)

for adsorptive filtration targeting the removal of toxic ions. (d) The AFM image of a monolayer MoS₂

nanosheet with a depth profile revealing a thickness of ~ 1.1 nm.

Selectivity of MoS₂ nanosheets towards different cations. To determine the selectivity of MoS₂ towards different cations, we first evaluated the adsorption of several toxic transition metal cations (Ni²⁺, Cd²⁺, Zn²⁺, Cu²⁺ and Pb²⁺) and some common background cations (Mg²⁺, K⁺, Ca²⁺) by MoS₂ monolayers in batch experiments (see details in Table S1 and S2). Figure 2a (blue hatched bars) shows the calculated removal of various cations in individual ion tests. MoS₂ nanosheets demonstrated nearly complete removal of Pb²⁺ and Cu²⁺ by effectively decreasing their concentrations from 5 mg/L, to 4 and 1 μ g/L respectively. In comparison, the removal efficiency was relatively high (~ 90%) for Cd²⁺, moderate (30 to 50%) for Zn²⁺, Ni²⁺ and Ca²⁺, and very low (< 20%) for Mg²⁺ and K⁺. In addition, the high affinity of MoS₂ nanosheets towards Pb²⁺ can be demonstrated by a low threshold concentration (0.1 mM) that induces visible aggregation of MoS₂ nanosheets within half an hour. While for poorly adsorbed ions (e.g., Mg²⁺), a higher threshold concentration for aggregation (0.5 mM) was observed (Figure S2).⁴²

To directly compare the affinity of MoS_2 nanosheets towards different cations in a competitive environment, we also conducted the adsorption experiments in an ion mixture containing all eight cations of the same concentration (~ 5 mg/L). As shown in Figure 2a (red unhatched bars), MoS_2 nanosheets maintained excellent removal of Pb^{2+} and Cu^{2+} by decreasing their concentrations from ~ 5 mg/L to a few micrograms per liter, which was in good agreement with those observed in individual ion tests. However, the removal of each of the other cation species was much lower than that when tested individually, indicating that the preferred adsorption of Cu^{2+} and Pb^{2+} significantly decreased the available sorption sites for other ions.

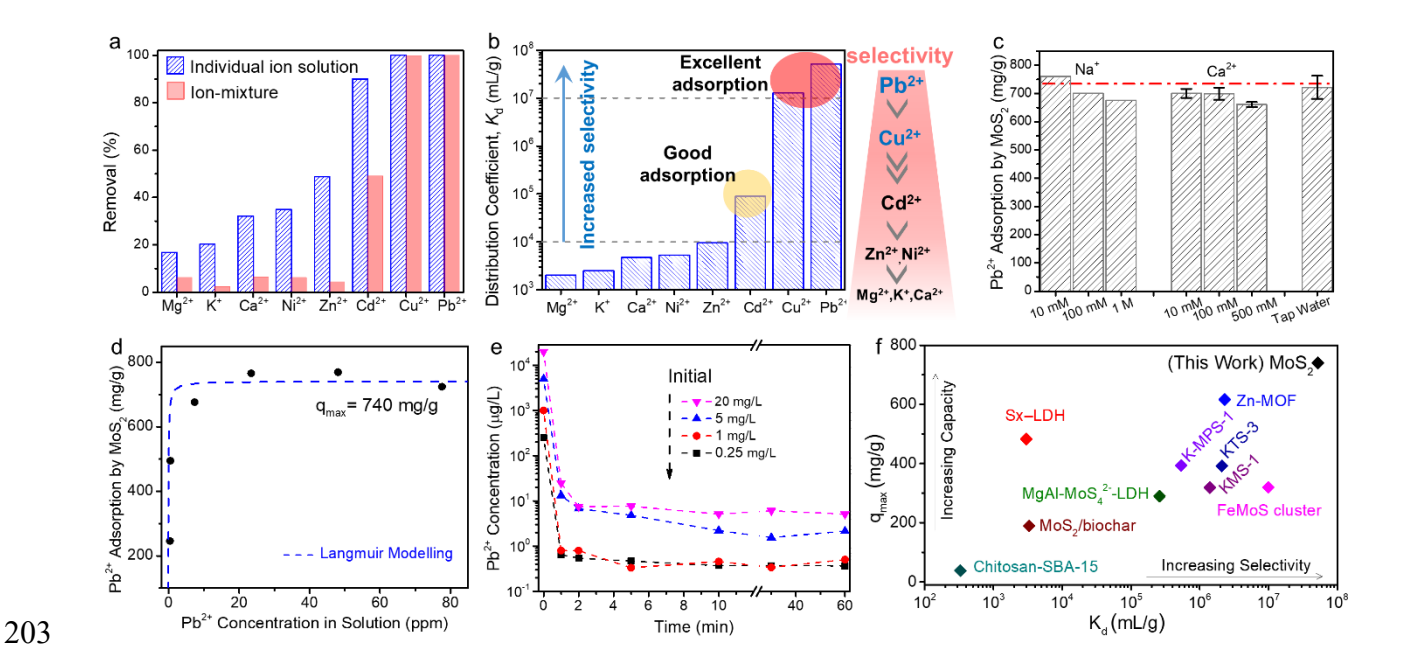


Figure 2. Characterization of the selectivity and capacity of Pb²⁺ adsorption by suspended MoS₂ nanosheets. (a) Removal of various cations by MoS₂ nanosheets in individual ion solutions and in a mixture containing all ions of equal concentration (5 mg/L). (b) Distribution coefficients K_d of various cation species. (c) Pb²⁺ removal by MoS₂ in the presence of Na⁺, Ca²⁺ or tap water impurities. The dashed line represents the maximum removal capacity observed in the pure water baseline experiment. (d) Isotherm of Pb²⁺ adsorption by MoS₂ fitted by Langmuir model (dash line). (e) Kinetics of Pb²⁺ adsorption at various initial Pb²⁺ concentrations. (f) Comparison of the adsorption capacity (q_{max}) and distribution coefficient (K_d) of MoS₂ nanosheets with those of other benchmark materials reported in the literature. (6, 11, 43-55)

The affinity of MoS₂ nanosheets to various cations can be compared by calculating their distribution coefficients K_d (Figure 2b). According to the individual cation test results, the K_d values of MoS₂ nanosheets for Pb²⁺ and Cu²⁺ are both >10⁷ mL/g, which are 2 to 4 orders of magnitude higher than those for other metal cations, revealing the excellent adsorptive selectivity of MoS₂ nanosheets towards Pb²⁺ and Cu²⁺. To further reveal the relative affinity of MoS₂ nanosheets to Pb²⁺ and Cu²⁺, we conducted competitive tests where the initial concentrations of Cu²⁺ and Pb²⁺ remained constant at ~ 5 mg/L, but the initial concentrations of MoS₂ nanosheets were reduced from 100 mg/L to 30, 15, and 5 mg/L, respectively. As shown in Figure S3 and Table S3, at lower concentrations (30 and 15 mg/L) of MoS₂ nanosheets, Pb²⁺ removal was still close to 100%, while the removal of Cu²⁺ decreased from 100% to 91.2% and 36.1% respectively. These

results indicate that when MoS_2 was limited in quantity, its adsorption sites highly preferred Pb^{2+} over Cu^{2+} . Only when the concentration of MoS_2 further decreased to 5 mg/L was there a slight decline in Pb^{2+} removal, whereas Cu^{2+} removal was very low (6.1%).

Overall, the MoS₂ monolayer displayed an adsorption affinity in the order $Pb^{2+} > Cu^{2+} >> Cd^{2+} > Zn^{2+}$, $Ni^{2+} > Mg^{2+}$, K^+ , Ca^{2+} (Figure 2b). This is consistent with the hard-soft principle in Lewis acid-base theory, i.e., the sulfur sites on MoS₂ offer strong soft-soft interactions towards soft acids (metal ions such as Pb^{2+} , Cu^{2+} , and Cd^{2+}). The high affinity/selectivity towards Pb^{2+} over hard acid species (Mg^{2+} , K^+ , Ca^{2+}) reveals the great promise of using MoS₂ nanosheets in the development of household POU devices for the removal of lead from drinking water. In addition, we tested the interference of Pb^{2+} adsorption by high concentrations of common cations (e.g., Na^+ and Ca^{2+}) that are ubiquitous in drinking water. We found that the presence of a high concentration of these background ions (up to 1 M NaNO₃, 1 M $Ca(NO_3)_2$, or concentrations characteristic of a tap water mimic, with detailed composition data in the Supporting Information) did not affect Pb^{2+} removal by MoS_2 (Figure 2c).

The Pb^{2+} adsorption capacity and kinetics were further studied to elucidate the removal mechanism. The adsorption of Pb^{2+} onto MoS_2 monolayers was examined by varying the initial Pb^{2+} concentration in the range of 25 to 150 mg/L. As shown in Figure 2d, the adsorption isotherm data can be better fitted by the Langmuir model than the Freundlich model (Figure S4), indicating the adsorption of a monolayer Pb^{2+} onto the MoS_2 nanosheet surface. According to the model, MoS_2 nanosheets have a maximum adsorption capacity of 740 mg/g toward Pb^{2+} (Figure 2d and Figure S5). The Pb^{2+} removal also depends on pH conditions (Figure S6). Higher removal capacity is found at neutral pH (\sim 740 mg/g) than at acidic conditions (e.g., \sim 350 mg/g at pH 3). The decrease in Pb^{2+} adsorption at lower pH indicates that the Pb^{2+} captured by MoS_2 may be attributed

to the ion exchange with protons on the nanosheets (H_{0.25}MoS₂),⁴⁰ the deprotonation of which is inhibited by low pH. Similar Pb²⁺ adsorption mechanisms and pH effects have been observed with other functional materials.^{43, 55} In this study, pH 6 was adopted to investigate the fundamental interactions between MoS₂ and Pb²⁺ in order to avoid the interference of possible hydroxide precipitate at alkaline conditions. Fast removal kinetics (2-3 logs Pb²⁺ removal within 2 min, as shown in Figure 2e) was observed regardless of initial Pb²⁺ concentration in solution (0.25 to 20 mg/L). The regeneration of MoS₂ can be achieved by using strong chelating agents with a formation constant higher than 10^{11.4} (Figure S7). In our study, EDTA with a formation constant of 10¹⁸ was chosen for regeneration. The regeneration of MoS₂ could maintain a 85-95% lead removal in 2 to 5 repeated regeneration cycles (Figure S8). The slight reduction in removal efficiency during regeneration was likely caused by the aggregation or partial oxidation of MoS₂ nanosheets.

Overall, the MoS₂ nanosheets studied in this work have superior lead adsorption capabilities compared with other materials reported so far. As shown in Figure 2f, our exfoliated MoS₂ nanosheets demonstrate a high Pb²⁺ adsorption capacity (740 mg/g) and an extremely high affinity K_d (5.2±1.9×10⁷ mL/g), outperforming previously reported materials including MOFs, layered metal sulfides, and sulfur-functionalized nanomaterials.^{6,11,43-49} Note that adsorbents with K_d values in the order of magnitude of 10⁴ are considered to have outstanding selectivity.⁵⁶ Examples include sulfur-based sorbents such as S_x - and MoS_4^2 --intercalated LDH (10³ to 2.6×10⁵ mL/g),^{11,46} layered metal sulfides (5.4×10⁵ to 2.1×10⁶ mL/g),^{43,47,49} MoS₂ hydrogel (1.32×10⁴ mL/g),⁵⁰ and others (10³-10⁵ mL/g).⁵³⁻⁵⁵ More details can be found in Table S4. The MoS₂ nanosheets indeed exhibit the highest K_d (10⁷ mL/g) among all materials to the best of our knowledge, demonstrating their excellent selectivity toward Pb²⁺.

Investigation of adsorption mechanism. To further elucidate the adsorption mechanisms, we

269 used DFT simulation based on first-principle calculations to study the interactions between metal 270 ions and 2H-MoS₂. 2H-MoS₂ was chosen for modelling because of its thermodynamic stability 271 and common presence in nature. As MoS₂ nanosheets are partially reduced during the 272 intercalation/exfoliation process, they are negatively charged and have a formula of H_{0.25}MoS₂ or MoS₂-0.25.40 According to this formula, we built a 4×4 MoS₂ supercell with 4 hydrogen atoms 273 274 evenly distributed on the surface (H₄(MoS₂)₁₆, Figure S14). Since all reactions take place in 275 aqueous solution, the ions are present in the hydrated form, and the number of water molecules in the hydration shell is determined based on literature data.⁵⁷ Therefore, the adsorption of a divalent 276 metal ion (M²⁺) onto MoS₂ can be described in equation 1. 277

$$278 \qquad H_4(MoS_2)_{16} + n[(H_2O)_4M^{2+}] \rightarrow [M_n(MoS_2)_{16}]^{2n-4} + 4[(H_2O)_2H^+] + (n-2)(H_2O)_4 \tag{1}$$

- where n varies in the range of 1 to 24 depending on the Pb/S coverage ratio ranging from 1/32 to
- 280 3/4. Accordingly, the corresponding free energy of adsorption ($\Delta G_{f,ads}$) is calculated by the
- 281 following equation:

$$282 \Delta G_{f,ads} = E_{[M_n(MoS_2)_{16}]^{2n-4}} + 4E_{(H_2O)_2H^+} + (n-2)E_{(H_2O)_4} - E_{H_4(MoS_2)_{16}} - nE_{(H_2O)_4M^{2+}} (2)$$

- 283 where E represents the internal energy of the corresponding compound, which can be obtained
- from the first-principle DFT calculations. A detailed illustration of the adsorption reaction and the
- 285 methodology used to calculate the free energy is discussed in the Supporting Information. A
- negative free energy $\Delta G_{f,ads}$ indicates that the adsorption is energetically favorable, and vice versa.

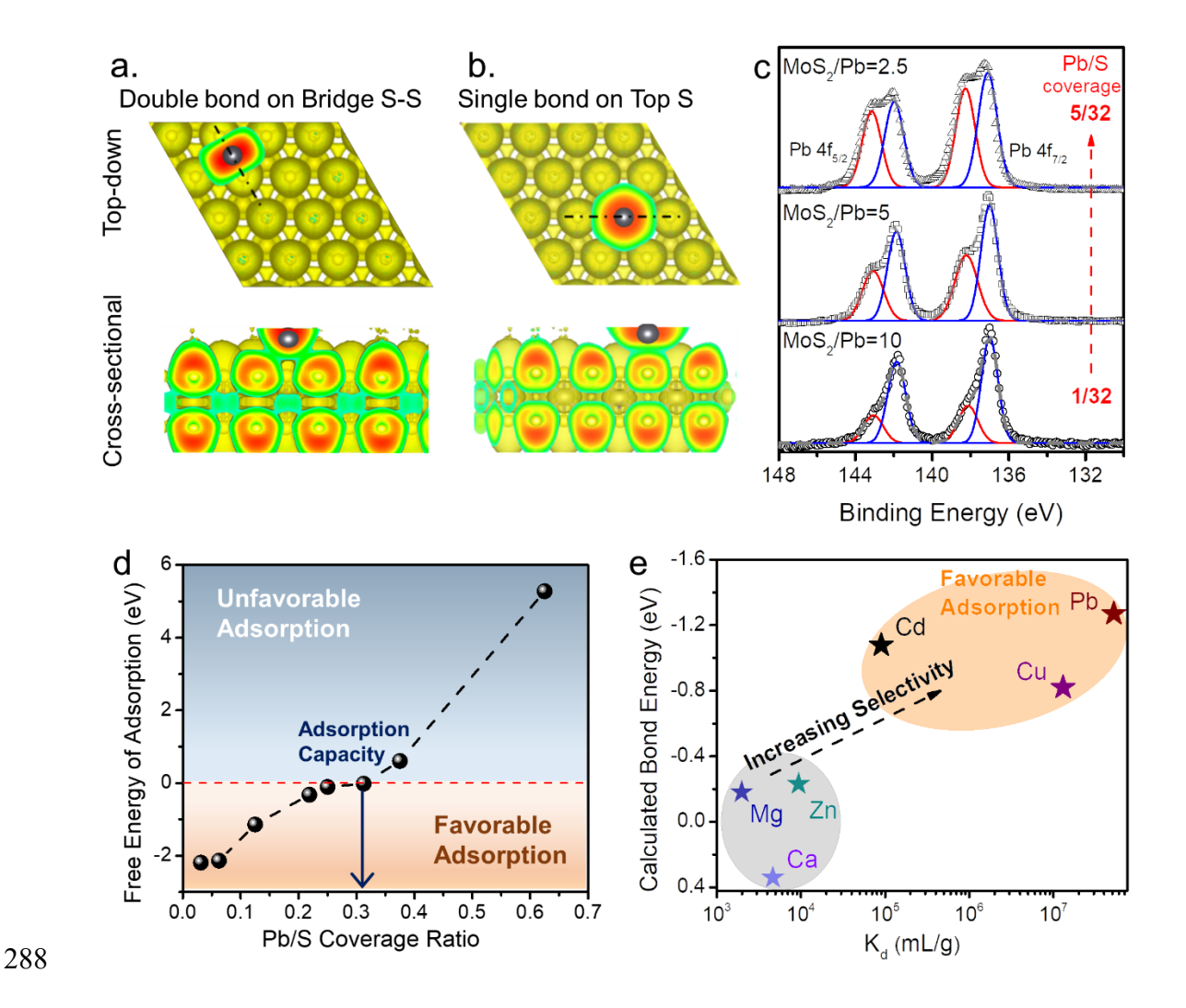


Figure 3. Mechanistic investigation of lead adsorption by DFT simulation and XPS spectra. The top-down and cross-sectional views of the electron localization function (ELF, with detailed explanation in Supporting Information) for the Pb-MoS₂ double bond formed on a bridge S-S site (a) and a single bond formed on a top-S site (b). (c) XPS spectra of Pb peaks with the Pb/S coverage ratio increasing from 1/32 to 5/32, which correspond to the MoS₂-Pb mass ratio ranging from 10 to 2.5 (see SI for calculation process). The peaks at higher (red) and lower (blue) binding energies are most likely attributed to single bonds on the top-S and double bonds on the bridge S-S sites, respectively. (d) The free energy of Pb²⁺ adsorption on MoS₂ surface as a function of Pb/S coverage ratio. (e) The maximum bond energy for the binding between cations and MoS₂.

The binding mechanisms between Pb^{2+} and MoS_2 nanosheets are affected by the Pb/S coverage ratio. The most stable (energetically favorable) binding site on MoS_2 is the Bridge S-S site (Figure 3a), where a Pb^{2+} binds to two neighboring S-atoms with an equal bond length of \sim 2.7 Å. However, when the Pb/S coverage ratio increases, the dominating binding site shifts to the Top-S site, where a Pb^{2+} binds to only one S atom with a bond length of \sim 2.5 Å (Figure 3b). The

Pb-MoS₂ double bond formed at the Bridge S-S position (binding energy of -1.3 eV) is stronger than the single bond at the Top-S position (binding energy of -1.0 eV). A more detailed description of the binding mechanism, formation energy, bond length, geometry, and effects of Pb-S coverage can be found in Tables S5 and S6, Figures S19 to S22. The simulation results are correlated with the deconvolution of Pb 4f peaks in the XPS spectra at different Pb/S coverage ratios. As shown in Figure 3c, when the Pb/S coverage ratio increases from 1/32 to 5/32 (i.e., the MoS₂/Pb mass ratio decreases from 10 to 2.5), the component peak at higher binding energy (red line) increases in strength, corresponding to more single bonds on Top-S sites, while the component peak at lower binding energy (blue line) becomes weaker, corresponding to less double bonds on the Bridge-S-S sites. The XPS results are consistent with the simulation results.

The overall free energy ($\Delta G_{f,ads}$) for Pb adsorption onto MoS₂ is strongly affected by the Pb/S coverage (Figure 3d). The free energy of adsorption increases with increasing Pb/S coverage ratio, indicating that the adsorption of Pb becomes weaker when more Pb is adsorbed onto MoS₂ surfaces. The free energy becomes positive when Pb/S coverage is over 0.31, demonstrating that the adsorption of more Pb beyond the 31% coverage is energetically unfavorable. The 31% coverage amounts to an adsorption capacity of 802 mg/g, which is very close to our experimental results (740 mg/g).

To understand the stronger selectivity towards Pb²⁺ than towards other cations, the binding energy for other cations were also calculated using the DFT model. The favorable binding mechanism for each metal species is shown in Table S7. It was found that for almost all divalent cations except Ca²⁺, the most stable (energetically favorable) binding mechanism is the double bond formed at Bridge S-S sites. The binding of Ca²⁺ is unique because the bonds on all binding sites exhibit a positive formation energy, indicating unfavorable adsorption. The formation energy

of the most favorable binding of each cation on the MoS₂ nanosheet is correlated with the experimentally measured K_d values in Figure 3e. In general, a negative formation energy of around -1 eV (for Pb²⁺, Cd²⁺, and Cu²⁺) corresponds to a high K_d value (above 10⁵ mL/g), demonstrating good consistency between simulation and experimental results. Among all metal ions analyzed, the formation energy of Pb-MoS₂ has the most negative value (-1.3 eV), indicating stronger bonding and more facile interactions of Pb²⁺ than those of Cu²⁺ and Cd²⁺ with MoS₂ nanosheets, consistent with its highest K_d value measured experimentally. The formation energy of Zn²⁺, Mg²⁺ and Ca²⁺ is much less negative or becomes positive (> - 0.4 eV), consistent with their low K_d values (below 10⁴ mL/g) measured experimentally.

It is worth noting that only 2H-MoS₂ was used to simulate the interactions between MoS₂ and metal ions, while the lab-synthesized MoS₂ nanosheets consisted of both 2H-MoS₂ and 1T-MoS₂. Although previous studies reported that 1T-MoS₂ is more functional in removing heavy metal than 2H-MoS₂,²² our 2H-MoS₂-based simulation was able to accurately predict the adsorption capacity and selectivity experimentally observed with mixed-phase MoS₂, indicating an insignificant phase effect. However, besides adsorption, metal ion removal can be potentially caused by redox reaction and/or precipitation formation with MoS₂ nanosheets or soluble molybdate species, in which case the phase of MoS₂ would play an important role. Nevertheless, more comprehensive experimental and simulation studies using both 2H-MoS₂ and 1T-MoS₂ are warranted to fully understand the phase effect.

To explore if redox reaction and/or precipitation are present in removing Pb²⁺ and other metal ions tested here, we carried out extensive XPS characterization of the metal-adsorbed MoS₂ samples (Pb-, Cu-, Cd-, Ni-, Zn-MoS₂). As shown in Figure S9a, compared to the pristine MoS₂, all metal-adsorbed MoS₂ samples exhibit similar Mo and S peak positions and intensities.

Meanwhile, the absence of oxidized S at 168 eV and constant 1T/2H ratios indicate no direct redox reaction occurring between MoS_2 and metal species tested here (Figure S9b and S9c). This is consistent with the previous findings that MoS_2 can not reduce Pb^{2+} or Cu^{2+} , although redox reaction contributes greatly to the removal of Ag^+ and Hg^{2+} that leads to oxidized S and reduced 1T/2H ratios.²⁶ We observed weak peaks of molybdate, which often co-exists in the MoS_2 suspension due to slow oxidative dissolution of MoS_2 by ambient oxygen. Based on the XPS characterization (Figure S9b), even if we assume all the molybdate contributes to Pb removal by forming precipitates, the precipitation accounts for less than ~ 10 % of the total Pb removal (see Supporting Information for calculation).

Layer-stacked MoS₂ as POU filter. Excellent capacity and selectivity are the pre-requisites for MoS₂ monolayers as potential building blocks for a POU filter. With these aspects demonstrated above, we further used MoS₂ monolayers to synthesize a layer-stacked MoS₂ membrane, and explored its potential for POU removal of lead from drinking water. The MoS₂ membranes were tested in filtration experiments with feed water containing various concentrations of Pb²⁺. The membrane maintained a constant water flux (145 L m⁻² h⁻¹ bar⁻¹) due to stable 2D nanochannels formed between stacked MoS₂ nanosheets with an interlayer distance of 1.2 nm (Figure S10). The interlayer spacing is large enough to allow Pb²⁺ to enter the 2D nanochannels in the MoS₂ membrane and adsorb it onto the channel walls. As a result, Pb²⁺ concentration is efficiently lowered from 0.25-3 mg/L in the feed water, to less than 10 μg/L in the effluent, which is the WHO guideline value. Since the MoS₂ membrane mainly removes Pb²⁺ by adsorption, there would be a breakthrough point when the effluent concentration rises above 10 μg/L. The total effluent volume at the breakthrough point defines the treatment capacity of the adsorptive membrane. As

shown in Figure 4a, when the Pb²⁺ concentration in feed water was 0.25, 1, and 3 mg/L, the treatment capacity of the MoS₂ membrane was 800, 180, and 70 mL, respectively. It is estimated that the residence time of Pb²⁺ in the MoS₂ membrane is merely 0.02 s (see calculation in Figure S10), so the breakthrough is most likely controlled by a dynamic process instead of reaching an equilibrium condition for adsorption. Therefore, the treatment capacity of MoS₂ membranes can be further improved by increasing the residence time, e.g., by synthesizing a thicker membrane (Figure S12).

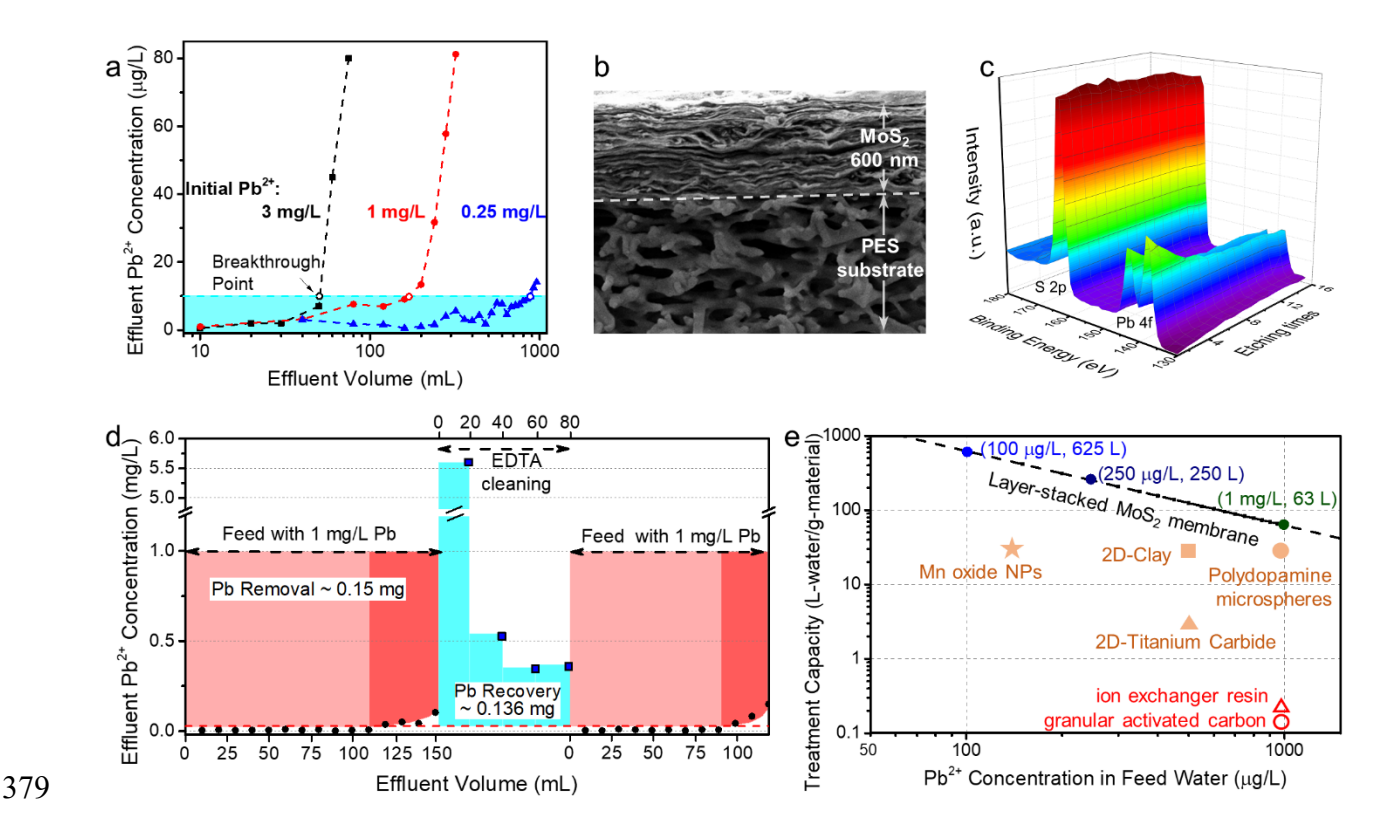


Figure 4. Layer-stacked MoS₂ membrane as a POU filter. (a) The performance of MoS₂ membranes in filtering a feed water containing 0.25 to 3 mg/L Pb^{2+} . The treatment capacity is defined as the total effluent volume at the breakthrough point, which was reached when the effluent Pb²⁺ concentration reached $10 \mu \text{g/L}$. The cross-sectional SEM (b) and XPS depth profile (c) of the MoS₂ membrane after filtering Pb²⁺ water (see Figure S11 for detailed peak intensity evolution). (d) The regeneration of MoS₂ membrane using EDTA cleaning. (e) Treatment capacities (L-water/g-material) of MoS₂ membranes and other adsorptive membranes reported in the literature. Membranes fabricated by commercial materials are represented by red hollow symbols, and those by lab-synthetic materials are represented by amber filled symbols.

SEM and XPS were used to characterize a used MoS₂ membrane after being tested with

1 mg/L Pb²⁺ feed solution and reaching the breakthrough point in filtration. The MoS₂ membrane maintains a stacked structure as shown in the cross-sectional SEM image (Figure 4b). The distribution of adsorbed lead in the MoS₂ membrane can be observed in the depth profile of the S 2p and Pb 4f peaks obtained by etching 300 nm (15 times × 20 nm etching depth) into the MoS₂ membrane during XPS characterization (Figure 4c). The Pb/S atomic ratio is high (12 %) on the membrane surface, and gradually decreases to around 5 % at 100 nm depth and below. The higher Pb content on the membrane top surface could be partially attributed to the diffusion of Pb²⁺ ions from water during drying. The relatively constant Pb/S ratio in the membrane interior confirms that adsorption instead of membrane exclusion is the dominant Pb²⁺ removal mechanism.

The regeneration ability of the MoS₂ membrane was evaluated by using EDTA cleaning to remove the adsorbed Pb^{2+} ions from the membrane after a filtration experiment. As shown in Figure 4d, the MoS₂ membrane adsorbed 0.15 mg Pb^{2+} from the first filtration cycle, and the EDTA cleaning by flushing with 80 mL EDTA solution recovered approximately 0.136 mg Pb^{2+} from the membrane, leading to a recovery of more than 90 %. It is worth noting that the concentration of recovered Pb^{2+} in the first 20 mL EDTA solution was as high as 5.5 mg/L, demonstrating the effectiveness in regenerating MoS_2 membranes. A second filtration cycle was performed after EDTA cleaning, and the regenerated MoS_2 membrane could reduce Pb^{2+} concentration to less than $10~\mu g/L$ with a treatment capacity of 90 mL, equivalent to nearly 90% of the original treatment capacity of a fresh MoS_2 membrane.

The treatment capacity of a POU filter is calculated by considering a conservative 65.6 mg/g lead removal capacity of the MoS₂ membrane (based on the tests shown in Figure S12). As shown in Figure 4e, the POU device demonstrates a treatment capacity of 63 to 625 L-water/g-MoS₂ depending on the initial Pb²⁺ concentration in tap water. For instance, when Pb²⁺

concentration in the water is 100 and 250 μ g/L, a POU device containing 1 g of MoS₂ membrane could effectively treat 625 and 170 L water, respectively. The treatment capacity of MoS₂ membrane is several orders of magnitude higher than that of adsorptive membranes made of commercial or lab-synthetic materials reported in the literature ^{12,58,59}. The superb performance can be attributed to the high adsorption capacity and selectivity of MoS₂ nanosheets as well as the fully accessible sulfur sites in the 1.2-nm 2D nanochannels enabled by the layer-stacking structure.

412

413

414

415

416

417

418

419

420

421

422

423

424

425

426

427

428

429

430

431

432

433

434

The leaching of MoS₂ nanosheets and soluble Mo species from MoS₂ membranes is also characterized in the filtration experiments. During the Pb adsorption and EDTA cleaning process, we observed a low concentration of leached Mo species (< 0.1 mg/L) in the filtrate (Figure S13). This is due to the slow oxidation of chemically exfoliated MoS₂ to soluble molybdate ions as was reported previously.⁶⁰ To the best of our knowledge, molybdate ions have not been reported to generate environmental toxicity or negative human health impacts at such low concentrations. The leaching problem can also be potentially addressed by using more stable MoS₂ prepared by ultrasonication, which significantly slows down Mo leaching (Figure S13). Loose nanosheets were not observed throughout all filtration tests, nor during a batch test where external pressure was removed, a condition that can accelerate nanosheet release if applicable (Figure S14). This structural stability is consistent with our previous finding that the strong vdW forces between MoS₂ nanosheets could potentially prevent the layer-stacked MoS₂ nanosheets from releasing in water.⁴¹ Environmental Implications. Our findings suggest that emerging 2D MoS₂ nanosheets can find important applications like lead removal from drinking water. MoS2's superb lead adsorption capabilities are evidenced by its adsorption capacity (740 mg/g) and its extremely high distribution coefficient K_d (5.2×10⁷ mL/g), both of which are among the highest for materials that have ever been reported to the best of our knowledge. Additionally, once assembled into a layer-stacked

membrane, the unique 1.2-nm 2D nanochannels formed between MoS₂ nanosheets make all the surface sulfur sites fully accessible for lead adsorption, while allowing water to permeate through the membrane at a fast speed. The layer-stacked MoS₂ membrane could effectively remove Pb²⁺ in drinking water from a few mg/L to less than 10 μg/L, with a treatment capacity a few orders of magnitude higher than that of membrane filters fabricated with commercial or other nanomaterials. An additional advantage of the MoS₂ membrane is that the nanochannels also enable the rejection of lead-containing particulates, a common form of lead contamination in tap water due to the corrosion of drinking water distribution pipes.⁶¹ MoS₂ has also been reported to have excellent antimicrobial/antifouling properties,^{62,63} another important feature for multi-functional membrane applications. With exfoliation and synthesis methodology maturing, the cost and complexity of MoS₂ nanosheet production is expected to continuously decrease. Therefore, we believe that MoS₂ membrane-based technology holds great promise as a POU device installed in households, schools, or public utilities to remediate lead contamination and safeguard drinking water quality for the public.

Associated Content

Supporting Information

The Supporting Information is available free of charge on the ACS Publications website. This document includes additional characterization of MoS₂ nanosheets and membranes, supplementary adsorption results, DFT modeling process and results.

Acknowledgements

456

466

- The material is based upon work supported by U.S. National Science Foundation (NSF) under
- award nos. CBET-1565452 and CBET-1706059. Work at the Molecular Foundry was supported
- by the Office of Science, Office of Basic Energy Sciences, of the U.S. Department of Energy under
- 460 contract no. DE-AC02-05CH11231. Work at SUSTech was supported by SUSTech-MIT Joint
- 461 Center for Mechanical Engineering Education and Research, and State Environmental Protection
- 462 Key Laboratory of Integrated Surface Water-Groundwater Pollution Control. The authors
- acknowledge the assistance of SUSTech Core Research Facilities. The opinions expressed herein,
- however, are those of the authors and do not necessarily reflect those of the sponsors. Z Wang and
- 465 Q Tu contributed equally to this work.

467 **References**

- Pieper, K. J.; Tang, M.; Edwards, M. A., Flint water crisis caused by interrupted
- 469 corrosion control: Investigating "ground zero" home. Environmental science & technology 2017,
- *470 51*, (4), 2007-2014.
- Pieper, K. J.; Nystrom, V. E.; Parks, J.; Jennings, K.; Faircloth, H.; Morgan, J. B.;
- Bruckner, J.; Edwards, M. A., Elevated lead in water of private wells poses health risks: Case
- study in macon county, north carolina. *Environmental science & technology* **2018**, *52*, (7), 4350-
- 474 4357.
- 475 3. US-EPA, Maximum contaminant level goals and national primary drinking water
- 476 regulations for lead and copper; final rule. In Federal Register: 1991.
- 477 4. WHO, Guidelines for drinking-water quality In World Health Organization: 1993.
- Ngueta, G.; Abdous, B.; Tardif, R.; St-Laurent, J.; Levallois, P., Use of a cumulative
- exposure index to estimate the impact of tap water lead concentration on blood lead levels in 1-to
- 5-year-old children (montréal, canada). Environmental Health Perspectives 2016, 124, (3), 388.
- 481 6. Yu, C.; Shao, Z.; Hou, H., A functionalized metal-organic framework decorated with o-
- groups showing excellent performance for lead (ii) removal from aqueous solution. *Chemical*
- 483 *Science* **2017**, *8*, (11), 7611-7619.
- Sun, D. T.; Peng, L.; Reeder, W. S.; Moosavi, S. M.; Tiana, D.; Britt, D. K.; Oveisi, E.;
- Queen, W. L., Rapid, selective heavy metal removal from water by a metal-organic
- 486 framework/polydopamine composite. ACS central science 2018, 4, (3), 349-356.
- 487 8. Zhao, G.; Li, J.; Ren, X.; Chen, C.; Wang, X., Few-layered graphene oxide nanosheets as
- superior sorbents for heavy metal ion pollution management. Environmental science &
- 489 *technology* **2011,** *45*, (24), 10454-10462.
- 490 9. Sun, Q.; Aguila, B.; Perman, J.; Earl, L. D.; Abney, C. W.; Cheng, Y.; Wei, H.; Nguyen,
- N.; Wojtas, L.; Ma, S., Postsynthetically modified covalent organic frameworks for efficient and
- 492 effective mercury removal. Journal of the American Chemical Society 2017, 139, (7), 2786-
- 493 2793.
- 494 10. Huang, N.; Zhai, L.; Xu, H.; Jiang, D., Stable covalent organic frameworks for
- 495 exceptional mercury removal from aqueous solutions. Journal of the American Chemical Society

- **2017,** *139*, (6), 2428-2434.
- 497 11. Ma, L.; Wang, Q.; Islam, S. M.; Liu, Y.; Ma, S.; Kanatzidis, M. G., Highly selective and
- efficient removal of heavy metals by layered double hydroxide intercalated with the mos₄²⁻ion.
- 499 *Journal of the American Chemical Society* **2016**, *138*, (8), 2858-2866.
- Peng, Q.; Guo, J.; Zhang, Q.; Xiang, J.; Liu, B.; Zhou, A.; Liu, R.; Tian, Y., Unique lead
- adsorption behavior of activated hydroxyl group in two-dimensional titanium carbide. Journal of
- 502 the American Chemical Society **2014**, 136, (11), 4113-4116.
- 503 13. Li, Z.; Fan, R.; Hu, Z.; Li, W.; Zhou, H.; Kang, S.; Zhang, Y.; Zhang, H.; Wang, G.,
- 504 Ethanol introduced synthesis of ultrastable 1t-mos₂ for removal of cr(vi). *Journal of Hazardous*
- 505 materials **2020**, 394, 122525.
- 506 14. Chen, Z.; Zhang, S.; Liu, Y.; Alharbi, N. S.; Rabah, S. O.; Wang, S.; Wang, X., Synthesis
- and fabrication of g-c₃n₄-based materials and their application in elimination of pollutants.
- 508 Science of the Total Environment **2020**, 139054.
- 509 15. Hu, B.; Ai, Y.; Jin, J.; Hayat, T.; Alsaedi, A.; Zhuang, L.; Wang, X., Efficient elimination
- of organic and inorganic pollutants by biochar and biochar-based materials. *Biochar* **2020**, *2*, (1),
- 511 47-64.
- 512 16. Wang, Z.; Mi, B., Environmental applications of 2d molybdenum disulfide (mos2)
- 513 nanosheets. Environmental Science & Technology 2017, 51, (15), 8229-8244.
- 514 17. Fausey, C. L.; Zucker, I.; Lee, D. E.; Shaulsky, E.; Zimmerman, J. B.; Elimelech, M.,
- 515 Tunable molybdenum disulfide-enabled fiber mats for high-efficiency removal of mercury from
- 516 water. ACS applied materials & interfaces **2020**, 12, (16), 18446-18456.
- 517 18. Ai, K.; Ruan, C.; Shen, M.; Lu, L., Mos₂ nanosheets with widened interlayer spacing for
- 518 high-efficiency removal of mercury in aquatic systems. Advanced Functional Materials 2016,
- 519 *26*, (30), 5542-5549.
- 520 19. Subrahmanyam, K. S.; Malliakas, C. D.; Sarma, D.; Armatas, G. S.; Wu, J.; Kanatzidis,
- M. G., Ion-exchangeable molybdenum sulfide porous chalcogel: Gas adsorption and capture of
- 522 iodine and mercury. Journal of the American Chemical Society 2015, 137, (43), 13943-13948.
- 523 20. Wang, J.; Zhang, W.; Yue, X.; Yang, Q.; Liu, F.; Wang, Y.; Zhang, D.; Li, Z.; Wang, J.,
- One-pot synthesis of multifunctional magnetic ferrite-mos₂-carbon dot nanohybrid adsorbent for
- efficient pb(ii) removal. Journal of Materials Chemistry A 2016, 4, (10), 3893-3900.
- 526 21. Zhao, H.; Yang, G.; Gao, X.; Pang, C. H.; Kingman, S. W.; Wu, T., Hg0 capture over
- 527 comos/γ-al₂o₃ with mos₂ nanosheets at low temperatures. *Environmental science & technology*
- **2016,** *50*, (2), 1056-1064.
- 529 22. Luo, J.; Fu, K.; Sun, M.; Yin, K.; Wang, D.; Liu, X.; Crittenden, J. C., Phase-mediated
- heavy metal adsorption from aqueous solutions using two-dimensional layered mos₂. ACS
- 531 applied materials & interfaces **2019**, 11, (42), 38789-38797.
- Zhang, L.; He, X.; Zhou, Q.; Hu, X., Fabrication of 1t-mos₂ nanosheets and the high-
- efficiency removal of toxic metals in aquatic systems: Performance and mechanisms. *Chemical*
- 534 Engineering Journal **2020**, *386*, 123996.
- 535 24. Kumar, N.; Fosso-Kankeu, E.; Ray, S. S., Achieving controllable mos₂ nanostructures
- with increased interlayer spacing for efficient removal of pb(ii) from aquatic systems. ACS
- 537 applied materials & interfaces **2019**, 11, (21), 19141-19155.
- 538 25. Li, D. O.; Gilliam, M. S.; Debnath, A.; Chu, X. S.; Yousaf, A.; Green, A. A.; Wang, Q.
- H., Interaction of pb²⁺ ions in water with two-dimensional molybdenum disulfide. *Journal of*
- 540 *Physics: Materials* **2020,** *3*, (2), 024007.
- Wang, Z.; Sim, A.; Urban, J. J.; Mi, B., Removal and recovery of heavy metal ions by

- 542 two-dimensional mos₂ nanosheets: Performance and mechanisms. *Environmental science* &
- 543 technology **2018**, *52*, (17), 9741-9748.
- 544 27. Joensen, P.; Crozier, E.; Alberding, N.; Frindt, R., A study of single-layer and restacked
- mos₂ by x-ray diffraction and x-ray absorption spectroscopy. *Journal of Physics C: Solid State*
- 546 *Physics* **1987,** *20*, (26), 4043.
- 547 28. Kresse, G.; Furthmüller, J., Efficient iterative schemes for ab initio total-energy
- calculations using a plane-wave basis set. *Physical Review B* **1996,** *54*, (16), 11169.
- 549 29. Perdew, J. P.; Burke, K.; Ernzerhof, M., Generalized gradient approximation made
- simple. *Physical Review Letters* **1996,** 77, (18), 3865.
- 551 30. Blöchl, P. E., Projector augmented-wave method. *Physical Review B* **1994**, *50*, (24),
- 552 17953.
- 553 31. Monkhorst, H. J.; Pack, J. D., Special points for brillouin-zone integrations. *Physical*
- 554 Review B **1976**, 13, (12), 5188.
- 555 32. Grimme, S.; Antony, J.; Ehrlich, S.; Krieg, H., A consistent and accurate ab initio
- parametrization of density functional dispersion correction (dft-d) for the 94 elements h-pu. *The*
- *Journal of chemical physics* **2010,** *132*, (15), 154104.
- 558 33. Silvi, B., The spin-pair compositions as local indicators of the nature of the bonding.
- *Journal of Physical Chemistry A* **2003**, *107*, (17), 3081-3085.
- 560 34. Gillespie, R. J.; Noury, S.; Pilmé, J.; Silvi, B., An electron localization function study of
- the geometry of d0 molecules of the period 4 metals ca to mn. *Inorganic Chemistry* **2004,** 43,
- 562 (10), 3248-3256.
- 563 35. Wu, M.; Yao, X.; Hao, Y.; Dong, H.; Cheng, Y.; Liu, H.; Lu, F.; Wang, W.; Cho, K.;
- Wang, W.-H., Electronic structures, magnetic properties and band alignments of 3d transition
- metal atoms doped monolayer mos₂. *Physics Letters A* **2018**, 382, (2-3), 111-115.
- 566 36. Chen, Y.-Y.; Dong, M.; Qin, Z.; Wen, X.-D.; Fan, W.; Wang, J., A dft study on the
- adsorption and dissociation of methanol over mos₂ surface. *Journal of Molecular Catalysis A:*
- 568 *Chemical* **2011,** *338*, (1-2), 44-50.
- 569 37. Ansari, R.; Shahnazari, A.; Malakpour, S.; Faghihnasiri, M.; Sahmani, S., A dft study on
- 570 the elastic and plastic properties of mos₂ nanosheet subjected to external electric field.
- 571 Superlattices and Microstructures **2016**, 97, 506-518.
- 572 38. Rasmussen, F. A.; Thygesen, K. S., Computational 2d materials database: Electronic
- 573 structure of transition-metal dichalcogenides and oxides. The Journal of Physical Chemistry C
- **2015,** *119*, (23), 13169-13183.
- 575 39. Eda, G.; Yamaguchi, H.; Voiry, D.; Fujita, T.; Chen, M.; Chhowalla, M.,
- 576 Photoluminescence from chemically exfoliated mos₂. Nano Letters **2011**, 11, (12), 5111-5116.
- Heising, J.; Kanatzidis, M. G., Exfoliated and restacked mos₂ and ws₂: Ionic or neutral
- 578 species? Encapsulation and ordering of hard electropositive cations. *Journal of the American*
- 579 *Chemical Society* **1999,** *121*, (50), 11720-11732.
- Wang, Z.; Tu, Q.; Zheng, S.; Urban, J. J.; Li, S.; Mi, B., Understanding the aqueous
- stability and filtration capability of mos₂ membranes. *Nano Letters* **2017**, *17*, (12), 7289-7298.
- 582 42. Yang, K.; Chen, B.; Zhu, X.; Xing, B., Aggregation, adsorption, and morphological
- transformation of graphene oxide in aqueous solutions containing different metal cations.
- *Environmental science & technology* **2016**, *50*, (20), 11066-11075.
- Rathore, E.; Pal, P.; Biswas, K., Layered metal chalcophosphate (k-mps-1) for efficient,
- selective, and ppb level sequestration of pb from water. The Journal of Physical Chemistry C
- **2017,** *121*, (14), 7959-7966.

- 588 44. Zhang, W.; Shi, S.; Zhu, W.; Yang, C.; Li, S.; Liu, X.; Hu, N.; Huang, L.; Wang, R.; Suo,
- Y., In-situ fixation of all-inorganic mo–fe–s clusters for the highly selective removal of lead (ii).
- 590 ACS applied materials & interfaces **2017**, 9, (38), 32720-32726.
- 591 45. Liu, Y.; Liu, Z.; Gao, J.; Dai, J.; Han, J.; Wang, Y.; Xie, J.; Yan, Y., Selective adsorption
- behavior of pb (ii) by mesoporous silica sba-15-supported pb (ii)-imprinted polymer based on
- 593 surface molecularly imprinting technique. Journal of Hazardous materials 2011, 186, (1), 197-
- 594 205.
- 595 46. Ma, S.; Chen, Q.; Li, H.; Wang, P.; Islam, S. M.; Gu, Q.; Yang, X.; Kanatzidis, M. G.,
- Highly selective and efficient heavy metal capture with polysulfide intercalated layered double
- 597 hydroxides. *Journal of Materials Chemistry A* **2014**, *2*, (26), 10280-10289.
- 598 47. Manos, M. J.; Kanatzidis, M. G., Sequestration of heavy metals from water with layered
- 599 metal sulfides. *Chemistry–A European Journal* **2009**, *15*, (19), 4779-4784.
- 600 48. Zhu, H.; Tan, X.; Tan, L.; Chen, C.; Alharbi, N. S.; Hayat, T.; Fang, M.; Wang, X.,
- Biochar derived from sawdust embedded with molybdenum disulfide for highly selective
- removal of pb $^{2+}$. ACS Applied Nano Materials **2018**, 1, (6), 2689-2698.
- 603 49. Sarma, D.; Islam, S. M.; Subrahmanyam, K.; Kanatzidis, M. G., Efficient and selective
- heavy metal sequestration from water by using layered sulfide $k_{2x}s_{14-x}s_{8-x}$ (x= 0.65–1; kts-3).
- 605 *Journal of Materials Chemistry A* **2016**, *4*, (42), 16597-16605.
- 50. Zhuang, Y.-T.; Zhang, X.; Wang, D.-H.; Yu, Y.-L.; Wang, J.-H., Three-dimensional
- molybdenum disulfide/graphene hydrogel with tunable heterointerfaces for high selective hg (ii)
- scavenging. Journal of Colloid and Interface Science 2018, 514, 715-722.
- 51. Zhou, L.; Ji, L.; Ma, P.-C.; Shao, Y.; Zhang, H.; Gao, W.; Li, Y., Development of carbon
- 610 nanotubes/cofe₂o₄ magnetic hybrid material for removal of tetrabromobisphenol a and pb (ii).
- 611 *Journal of Hazardous materials* **2014,** *265*, 104-114.
- 612 52. Guo, X.; Du, B.; Wei, Q.; Yang, J.; Hu, L.; Yan, L.; Xu, W., Synthesis of amino
- functionalized magnetic graphenes composite material and its application to remove cr (vi), pb
- 614 (ii), hg (ii), cd (ii) and ni (ii) from contaminated water. Journal of Hazardous materials 2014,
- 615 *278*, 211-220.
- 53. Yantasee, W.; Warner, C. L.; Sangvanich, T.; Addleman, R. S.; Carter, T. G.; Wiacek, R.
- J.; Fryxell, G. E.; Timchalk, C.; Warner, M. G., Removal of heavy metals from aqueous systems
- with thiol functionalized superparamagnetic nanoparticles. Environmental science & technology
- 619 **2007,** *41*, (14), 5114-5119.
- 620 54. Manos, M. J.; Petkov, V. G.; Kanatzidis, M. G., $H_{2x}mn_xsn_{3-x}s_6$ (x= 0.11–0.25): A novel
- reusable sorbent for highly specific mercury capture under extreme ph conditions. Advanced
- 622 Functional Materials **2009**, 19, (7), 1087-1092.
- 623 55. Hassanzadeh Fard, Z.; Islam, S. M.; Kanatzidis, M. G., Porous amorphous chalcogenides
- as selective adsorbents for heavy metals. *Chemistry of Materials* **2015**, *27*, (18), 6189-6192.
- 625 56. Fryxell, G. E.; Lin, Y.; Fiskum, S.; Birnbaum, J. C.; Wu, H.; Kemner, K.; Kelly, S.,
- 626 Actinide sequestration using self-assembled monolayers on mesoporous supports. *Environmental*
- 627 science & technology **2005**, 39, (5), 1324-1331.
- 628 57. Wander, M. C.; Clark, A. E., Hydration properties of aqueous pb (ii) ion. *Inorganic*
- 629 Chemistry **2008**, 47, (18), 8233-8241.
- 58. Zhang, Q.; Yang, Q.; Phanlavong, P.; Li, Y.; Wang, Z.; Jiao, T.; Peng, Q., Highly efficient
- lead (ii) sequestration using size-controllable polydopamine microspheres with superior
- application capability and rapid capture. ACS Sustainable Chemistry & Engineering 2017, 5, (5),
- 633 4161-4170.

- 634 59. Yan, Z.; Fu, L.; Yang, H., Functionalized 2d clay derivative: Hybrid nanosheets with
- unique lead sorption behaviors and interface structure. Advanced Materials Interfaces 2018, 5,
- 636 (4), 1700934.
- 637 60. Wang, Z.; von dem Bussche, A.; Qiu, Y.; Valentin, T. M.; Gion, K.; Kane, A. B.; Hurt, R.
- H., Chemical dissolution pathways of mos₂ nanosheets in biological and environmental media.
- 639 Environmental science & technology **2016**, *50*, (13), 7208–7217.
- 640 61. Pieper, K.; Martin, R. L.; Tang, M.; Walters, L.; Parks, J.; Roy, S.; Devine, C. L.;
- Edwards, M. A., Evaluating water lead levels during the flint water crisis. *Environmental science*
- 642 & technology **2018**, *52*, (15), 8124-8132.
- 643 62. Yang, X.; Li, J.; Liang, T.; Ma, C.; Zhang, Y.; Chen, H.; Hanagata, N.; Su, H.; Xu, M.,
- Antibacterial activity of two-dimensional mos₂ sheets. *Nanoscale* **2014**, *6*, (17), 10126-10133.
- 645 63. Alam, I.; Guiney, L. M.; Hersam, M. C.; Chowdhury, I., Antifouling properties of two-
- dimensional molybdenum disulfide and graphene oxide. *Environmental Science: Nano* **2018,** 5,
- 647 (7), 1628-1639.